Morphometric changes in the human pulmonary acinus during inflation

A. J. Hajari, D. A. Yablonskiy, A. L. Sukstanskii, J. D. Quirk, M. S. Conradi and J. C. Woods

J Appl Physiol 112:937-943, 2012. First published 17 November 2011;
doi:10.1152/japplphysiol.00768.2011

J Appl Physiol 112: 937–943, 2012.
First published November 17, 2011; doi:10.1152/japplphysiol.00768.2011.

Morphometric changes in the human pulmonary acinus during inflation

A. J. Hajari,[1] D. A. Yablonskiy,[1,2] A. L. Sukstanskii,[2] J. D. Quirk,[2] M. S. Conradi,[1,2] and J. C. Woods[1,2]
Departments of [1]Physics and of [2]Radiology, Washington University, St. Louis, Missouri

Submitted 20 June 2011; accepted in final form 14 November 2011

Hajari AJ, Yablonskiy DA, Sukstanskii AL, Quirk JD, Conradi MS, Woods JC. Morphometric changes in the human pulmonary acinus during inflation. *J Appl Physiol* 112: 937–943, 2012. First published November 17, 2011; doi:10.1152/japplphysiol.00768.2011.—Despite decades of research into the mechanisms of lung inflation and deflation, there is little consensus about whether lung inflation occurs due to the recruitment of new alveoli or by changes in the size and/or shape of alveoli and alveolar ducts. In this study we use in vivo ^{3}He lung morphometry via MRI to measure the average alveolar depth and alveolar duct radius at three levels of inspiration in five healthy human subjects and calculate the average alveolar volume, surface area, and the total number of alveoli at each level of inflation. Our results indicate that during a 143 ± 18% increase in lung gas volume, the average alveolar depth decreases 21 ±5%, the average alveolar duct radius increases 7 ± 3%, and the total number of alveoli increases by 96 ± 9% (results are means ± SD between subjects; $P < 0.001$, $P < 0.01$, and $P < 0.00001$, respectively, via paired *t*-tests). Thus our results indicate that in healthy human subjects the lung inflates primarily by alveolar recruitment and, to a lesser extent, by anisotropic expansion of alveolar ducts.

MRI; ^{3}He; lung; morphometry; diffusion; inflation

IN RECENT YEARS pulmonary MRI experiments employing hyperpolarized gases such as ^{3}He (5, 10, 22, 25, 27, 32, 34) and ^{129}Xe (18, 20, 21) have proven important tools for performing noninvasive quantitative studies of lung microstructure. ^{3}He lung morphometry has been validated by comparison with histological measurements in humans (32, 34), mice (19, 30), and dogs (13) and has been used to quantitatively characterize changes in lung microstructure at various stages of emphysema in vivo in human subjects (23). Recently ^{3}He lung morphometry was used to study changes in lung microstructure during deflation in nonfixed excised canine lungs (13). Most studies of lung micromechanics before this were performed either by histology (3, 7, 9, 14, 17, 26, 29) or subpleural microscopy (1, 4, 6, 8), with conflicting conclusions. Despite over 50 years of research into the topic, there is still no consensus about whether lung inflation occurs due to changes in the size and/or shape of alveoli and alveolar ducts or by the recruitment of new alveoli.

The discrepancies in conclusions are likely due, in part, to shortcomings in the methods of investigation. Histological studies suffer from tissue alteration during the fixation process and an inability to reproduce the same measurements at different states of inflation/deflation in the same lung. Interpretations of the results of histological studies can also be unclear. Macklem (16) points out that plots of surface area vs. total lung volume from two different histology studies by Forrest (9) and Dunnill (7) could both be explained equally well by either isotropic expansion of alveolar ducts or alveolar recruitment. While in vivo subpleural microscopy overcomes the drawbacks of fixation, its measurements are restricted to alveoli just below the pleural surface, and it is possible that these alveoli behave differently from those in the bulk of the lung (1, 4). In addition, both methods sample only a small subset of total alveoli and require inferences of a complex three-dimensional structure from a two-dimensional measurement. Furthermore, neither method is suitable for in vivo studies of human lungs.

As a tool for studying lung micromechanics, ^{3}He lung morphometry is advantageous because it takes into account three-dimensional structure, samples all ventilated parts of the lung, and is spatially resolved. The technique employs a multiple *b*-value (multiple gradient strength) ^{3}He diffusion MRI experiment to measure anisotropic diffusion of hyperpolarized ^{3}He within alveolar ducts in images that cover the entire lung. Based on established relationships between anisotropic diffusion of helium within acinar airways and the alveolar duct geometry (27, 34), average values of alveolar duct radius, *R*, and alveolar depth, *h*, are obtained for the airways within each voxel of the MR image (Fig. 1). The results can be used to calculate the average surface area and volume of individual alveoli and alveolar duct units as well as the total number of alveoli (34). Furthermore, these experiments are safe and suitable for in vivo studies in humans (15).

The purpose of this study was to investigate how alveolar-duct geometry changes with lung inflation in vivo. Using ^{3}He lung morphometry we have, for the first time, measured microscopic alveolar geometrical parameters *R* and *h* (Fig. 1) in vivo in healthy human subjects at multiple lung volumes. We present here parameter maps and average values of the alveolar duct radius, *R*, alveolar depth, *h,* average alveolar duct surface area and volume, and the total number of alveoli at three different points during inspiration in five human subjects.

METHODS

Five healthy subjects (2 men, 3 women) between the ages of 22 and 32 yr (mean age 27 ± 4 yr) received proton and multiple *b*-value ^{3}He diffusion MRI scans at three distinct and reproducible lung volumes. Scans at each lung volume were acquired during a breath-hold following a breathing routine specific to each volume. Low lung volume scans were acquired by instructing the subject to exhale fully to residual volume (RV) and then inhale the contents of a 1-liter bag filled with either air (for proton scans) or a ^{3}He/N_2 mixture (for ^{3}He scans). After breathing in the bag's contents, the MR scan was immediately initiated and the subject held his/her breath for the duration of the scan (~9 s). Medium lung volume scans were obtained in a similar manner, but the 1-liter gas mixture was administered immediately after expiration during a resting breathing cycle (adding 1 liter from functional residual capacity, FRC). High lung volume scans were acquired by having the subject breath in the 1-liter gas mixture immediately after expiration during a resting breathing cycle and then continue to inhale room air until total lung capacity (TLC) was achieved. In this way proton and ^{3}He diffusion MR images were obtained at volumes corresponding to residual volume + 1 liter (RV + 1), functional residual capacity + 1 liter (FRC + 1), and total lung capacity (TLC).

Address for reprint requests and other correspondence: J. C. Woods, Washington Univ., Radiology, 299 S. Euclid Ave., Barnard Bldg. Rm 3350, St. Louis, MO 63110 (e-mail: Jason.woods@wustl.edu).

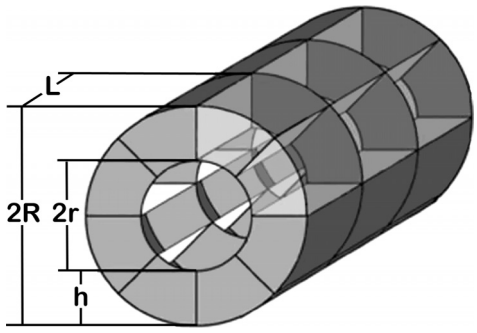

Fig. 1. Model of alveolar duct showing three alveolar duct units. The outer walls of the alveoli in the top right quadrant have been made transparent for clarity. See *Geometric model of alveolar ducts* for details.

All measurements of total lung volume were made from higher resolution two-dimensional multislice axial proton images (128 × 128; resolution = 3.52 × 3.52 × 15 mm; 21 slices completely covering both lungs from each subject) by semiautomated segmentation with the image processing program ImageJ (National Institutes of Health). Armstrong et al. report that at FRC tissue accounts for 19% of total lung volume (2). For each subject, 1 liter was subtracted from the measured lung volume at FRC + 1, and 19% of this value was taken as the lung tissue volume for that subject. This tissue volume was subtracted from each lung volume (RV + 1, FRC + 1, TLC), and an additional 150 ml was subtracted to account for conductive airspace volume (31), so that all reported volume measurements represent gas volume of the diffusion region of the lungs. In order to determine the reproducibility of the breathing routines, each routine was repeated five additional times at each of the three volumes (TLC, FRC + 1, and RV + 1) in *subjects 1* and *2*. Proton images were acquired following each of these additional breathing routines, and the volume was measured in the manner described above. The standard deviations of the five additional measurements at each lung volume are reported in Table 1 and demonstrate excellent reproducibility of the lung volumes.

Axial two-dimensional ^{3}He diffusion images (64 × 40; resolution = 7 × 7 × 30 mm; 3 slices) were acquired with a multiple *b*-value gradient echo pulse sequence using a custom-built ^{3}He volume-transmit/8-channel receiver pair (Stark Contrast MRI Coils Research, Erlangen, Germany). All images were obtained on a 1.5-T Siemens Magnetom Sonata scanner (Siemens Medical Systems, Iselin, NJ). Hyperpolarized ^{3}He gas was prepared using spin-exchange optical pumping with a commercial IGI.9600.He ^{3}He polarizer (GE Healthcare, Durham, NC). Nuclear spin polarization was ~35% for all experiments. All ^{3}He/N_2 gas mixtures contained ~0.3 liters of ^{3}He and 0.7 liters of N_2. Exhaled gas was captured in a helium-impermeable bag for ^{3}He recycling. All procedures were performed with IRB approval and ^{3}He IND exemption. Written informed consent was obtained from all subjects before participation in the study.

Geometric model of alveolar ducts (34). In our approach the lung acini are treated, in the framework proposed by Weibel and colleagues (12, 24), as networks of cylindrical airways covered with alveoli. An alveolar duct is modeled as a long hollow cylinder of radius R lined with annuli of inner radius r and outer radius R, periodically spaced along the inside of the cylinder and separated by a distance L. The space between the annuli is further segmented by eight alveolar walls extending between annuli and from the outer wall of the cylinder radially inward to a depth $h = R - r$ (see Fig. 1) (12).

Table 1. *^{3}He morphometry results*

	Volume, liters	R, μm	h, μm	S_a, $mm^2 \times 10^{-2}$	V_a, $mm^3 \times 10^{-3}$	N_{tot}, 10^6	ADC, cm^2/s
				Subject 1			
TLC	6.06 ± 0.17	325 ± 18	120 ± 24	17.3 ± 2.5	10.4 ± 1.5	594 ± 86	0.24 ± 0.03
FRC + 1	3.46 ± 0.09	322 ± 29	157 ± 37	20.1 ± 4.9	10.2 ± 2.8	358 ± 88	0.20 ± 0.03
RV + 1	2.59 ± 0.04	317 ± 32	169 ± 40	20.6 ± 5.3	9.9 ± 3.1	284 ± 79	0.18 ± 0.04
				Subject 2			
TLC	5.23 ± 0.02	318 ± 22	130 ± 20	17.7 ± 2.5	9.8 ± 1.2	536 ± 66	0.22 ± 0.02
FRC + 1	3.55 ± 0.03	307 ± 20	153 ± 24	18.4 ± 2.8	8.8 ± 1.4	412 ± 61	0.18 ± 0.02
RV + 1	2.26 ± 0.04	302 ± 24	167 ± 29	19.0 ± 3.8	8.4 ± 2.0	281 ± 61	0.16 ± 0.02
				Subject 3			
TLC	5.29	324 ± 22	158 ± 28	20.3 ± 3.6	10.4 ± 2.0	526 ± 93	0.20 ± 0.02
FRC + 1	3.38	307 ± 27	179 ± 33	20.4 ± 4.4	8.9 ± 2.2	397 ± 85	0.16 ± 0.02
RV + 1	2.02	300 ± 30	193 ± 37	20.6 ± 5.0	8.3 ± 2.4	262 ± 81	0.13 ± 0.02
				Subject 4			
TLC	5.91	324 ± 20	141 ± 23	19.0 ± 2.9	10.3 ± 1.8	585 ± 98	0.22 ± 0.02
FRC + 1	3.45	314 ± 20	152 ± 25	19.0 ± 3.2	9.4 ± 1.7	377 ± 70	0.19 ± 0.02
RV + 1	2.58	303 ± 24	173 ± 31	19.6 ± 3.8	8.5 ± 1.9	315 ± 76	0.16 ± 0.02
				Subject 5			
TLC	5.90	318 ± 21	139 ± 15	19.1 ± 3.3	9.8 ± 2.0	621 ± 108	0.20 ± 0.03
FRC + 1	4.26	308 ± 22	161 ± 11	19.3 ± 3.4	8.9 ± 1.8	495 ± 97	0.17 ± 0.02
RV + 1	2.21	289 ± 28	177 ± 11	19.1 ± 4.1	7.4 ± 1.9	321 ± 159	0.13 ± 0.02
				Average			
TLC	5.68	322 ± 3	135 ± 14	18.7 ± 3.0	10.1 ± 0.3	572 ± 40	0.22 ± 0.02
FRC + 1	3.62	311 ± 6	153 ± 11	19.4 ± 3.8	9.2 ± 0.6	408 ± 53	0.18 ± 0.02
RV + 1	2.33	302 ± 10	167 ± 11	19.8 ± 4.4	8.5 ± 0.9	293 ± 25	0.15 ± 0.02

Values for alveolar duct radius, R, alveolar depth, h, alveolar surface area, S_a, alveolar volume, V_a, total number of alveoli, N_{tot}, and apparent diffusion coefficient (ADC) for *subjects 1-5* at total lung capacity (TLC), functional residual capacity +1 liter (FRC + 1), and residual volume +1 liter (RV + 1) averaged over all voxels. Values are reported as averages ± SD. The last three rows are averages of mean results from all lungs ± SD in the means. The SD obtained from volume measurements from 5 additional proton scans at each volume are reported for *subjects 1* and *2*.

A single alveolar duct unit is defined as the space between two adjacent annuli and contains eight alveoli (see Ref. 34 for discussion regarding the number of alveoli per duct unit); the surface area of a single alveolus is

$$S_a = \frac{1}{4}\pi RL + \frac{1}{4}\pi(R^2 - r^2) + 2hL \quad (1)$$

and the volume of a single alveolus is

$$V_a = \frac{1}{8}\pi R^2 L \quad (2)$$

Note that the alveolar volume, as defined in *Eq. 2*, is one-eighth of the volume of the alveolar duct unit. That is, the alveolar volume includes both the alveolar proper volume (defined in *Eq. 3*) and one-eighth of the lumen volume (*Eq. 4*).

$$V_{a,proper} = \frac{1}{8}\pi(R^2 - r^2)L \quad (3)$$

$$V_{a,lumen} = \frac{1}{8}\pi r^2 L \quad (4)$$

Diffusion sequence and image analysis. ^{3}He diffusion within an alveolar duct is restricted by the airway walls. Within these cylindrical acinar airways, the diffusion is anisotropic and can be described by two distinct diffusion coefficients, D_T and D_L, which correspond to diffusion in the cylinder's transverse and longitudinal directions (27, 33). The apparent diffusion coefficient (ADC) is calculated from the anisotropic diffusion coefficients, D_T and D_L, by the relationship given in *Eq. 5*:

$$\mathrm{ADC} = \frac{1}{3}D_L + \frac{2}{3}D_T \quad (5)$$

The ^{3}He diffusion sequence used in this study incorporates a bipolar trapezoidal diffusion-sensitizing gradient characterized by a ramp time τ, pulse duration δ, pulse separation Δ, and maximum gradient strength G_m (33). ^{3}He MR signal attenuation due to diffusion within a single alveolar duct with long axis at an angle θ relative to the direction of the diffusion gradient is given by

$$S_{duct} = S_0 \exp\ [-b(D_L\cos^2\theta + D_T\sin^2\theta)] \quad (6)$$

where S_0 is the MR signal in the absence of a diffusion gradient, and b is the diffusion sensitizing parameter that depends solely on the diffusion gradient parameters (*Eq. 7*).

$$b = (\gamma G_m)^2\,[\delta^2(\Delta - \frac{\delta}{3}) + \tau(\delta^2 - 2\Delta\delta + \Delta\tau - \frac{7}{6}\delta\tau + \frac{8}{15}\tau^2)] \quad (7)$$

A typical imaging voxel contains thousands of randomly oriented alveolar ducts such that the net signal from any particular voxel is obtained by integrating *Eq. 6* uniformly over all orientations giving (33):

$$S_{voxel} = S_0 e^{-bD_T}\ (\frac{\pi}{4b(D_L - D_T)})^{1/2}\mathrm{erf}[b(D_L - D_T)]^{1/2} \quad (8)$$

where erf is the error function. The value of b is varied by changing the gradient amplitude, G_m, while all diffusion gradient timing parameters are kept constant (τ = 0.3 ms, $\delta = \Delta$ = 1.8 ms). Six diffusion-weighted images were obtained for each slice using b-values equal to 0, 2, 4, 6, 8, and 10 s/cm^2. The anisotropic diffusion coefficients are related to the geometric parameters R and h by the set of empirical equations determined by computer simulations described by Refs. 27 and 34. For each voxel, *Eq. 8* and equations A3–A5 from Ref. 34 are fit to the diffusion attenuated signal for the six b-values in order to obtain the mean alveolar duct radius, R, and the mean alveolar depth, h. In our geometric model of alveoli, we assume that there are eight alveoli around the duct and that the alveolar dimensions are the same in the direction along the airway axis and along the outer perimeter circumference such that the alveolar length is given by $L = 2R\sin(\pi/8)$ as suggested by Yablonskiy et al. (34). Using the geometric parameters R and h determined by ^{3}He lung morphometry, the alveolar surface area, S_a, and volume, V_a, are calculated from *Eqs. 1* and *2*. The alveolar number density, n_a, for a voxel containing alveoli with mean volume V_a is $n_a = 1/V_a$, and the total number of alveoli, N_{tot}, is the product of the average value of n_a over the entire lung and the total lung volume, $N_{tot} = \bar{n}_a \cdot V_{tot}$. The total lung surface area is $S_{tot} = N_{tot} \cdot S_a$.

For each pair of lungs at each volume, the values of R, h, S_a, V_a, n_a, and ADC from all voxels included in the analysis were each averaged. The statistical significance of the effects of lung volume on all parameters was determined for all five subjects by performing repeated-measures analysis of variance (ANOVA). P values < 0.05 were considered statistically significant.

RESULTS

All images demonstrated signal-to-noise more than sufficient (>100) to confidently fit the mathematical model to the data in order to obtain the geometric parameters R and h (the vast majority of imaging voxels within the lung had SNR > 100, typified by Fig. 2). N_{tot} and average values of R, h, S_a, V_a, and ADC for each pair of lungs at TLC, FRC + 1, and RV + 1 are given in Table 1. Image voxels with signal-to-noise less than 100 (28), containing large conducting airways (that is, with apparent diffusion coefficients greater than 0.5 cm^2/s), or with poor fitting confidence were excluded from the analysis and the reported averages. After excluding voxels containing large airways and with low signal-to-noise, fewer than 2% of voxels were excluded due to poor fitting confidence. Typical parameter maps of h and R are shown in Fig. 2. Each lung showed statistically significant microgeometrical changes with inflation across all volumes in R ($P < 0.001$), h ($P < 10^{-5}$), V_a ($P < 0.001$), N_{tot} ($P < 10^{-5}$), and ADC ($P < 10^{-6}$) via repeated-measures ANOVA. On average a 143 ± 18% increase in lung gas volume(from RV + 1 to TLC) led to a 7 ± 3% increase in the average alveolar duct radius, R, a 21 ± 5% decrease in alveolar depth, h, a 19 ± 10% increase in alveolar volume, V_a, a 96 ± 9% increase in the number of alveoli, N_{tot}, and a 41 ± 8% increase in ADC (results are averages ± SD; $P < 0.001$, $P < 10^{-5}$, $P < 0.001$, $P < 10^{-5}$, and $P < 10^{-5}$, respectively, via paired t-tests). All other pairwise comparisons of R, h, V_a, and N_{tot} were also significant ($P < 0.05$). There were no significant changes in the average alveolar surface area, S_a, between any of the three volumes ($P > 0.05$). P values for all statistical tests are reported in Table 2.

The standard deviations of the five additional proton image volume measurements at each lung volume for *subjects 1* and *2* are reported in Table 1. The average standard deviation for each of these six sets of measurements was 50 ml (1.1%) and the maximum standard deviation was 169 ml (2.4%), demonstrating excellent reproducibility of the lung volumes.

In Fig. 3, N_{tot} and average values of R, h, V_a, $V_{a,prop}$, $V_{a,lumen}$, and S_a for all five subjects at each of the three volumes TLC, FRC + 1, and RV + 1 are each plotted against total lung gas volume, V_{tot}. Each data point represents the average parameter value over the entire lung for a single subject at the lung volume indicated by the horizontal axis. In Fig. 4, total lung

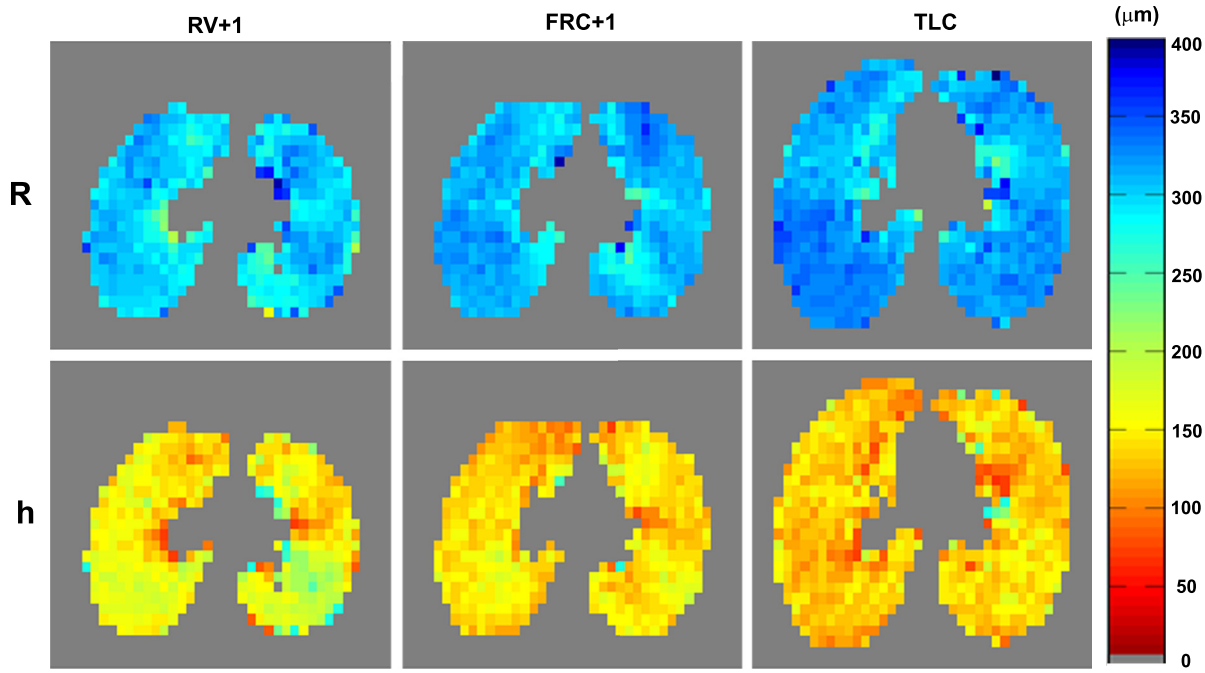

Fig. 2. Axial parameter maps of alveolar duct radius, *R* (top row), and alveolar depth, *h* (bottom row), from *slice 2* of *subject 5* at residual volume + 1 liter (RV + 1), functional residual capacity + 1 liter (FRC + 1), and total lung capacity (TLC) (*left* to *right*). The value of each voxel in the above parameter maps represents the average value of *R* (top row) and *h* (bottom row) of all acinar airways within that voxel as determined by the multiple *b*-value diffusion MR images.

surface area, S_{tot}, is plotted against V_{tot} and the power function given in *Eq. 9* is fit to the data.

DISCUSSION

In their chapter on micromechanics of the lung in the *Handbook of Physiology*, Greaves, Hildebrandt, and Hoppin (11) discuss five possible mechanisms of lung expansion. They propose that during inflation alveolar ducts might undergo: *1*) isotropic changes in alveolar dimensions (that is, uniform scaling of all dimensions), *2*) an increase in alveolar depth (a "saucer-to-cup"-like change in the shape of alveoli), *3*) a decrease in alveolar depth (a "cup-to-saucer"-like change in the shape of alveoli), *4*) no change in alveolar surface area (a special case of *3,* which the authors refer to as "accordion-like extension"), or *5*) instantaneous opening of new alveoli from a completely collapsed state via recruitment. An example of collapsed alveoli can be seen in Fig. 3 of Ref. 3 (left lower corner in panel A).

Our results in Fig. 3*C* show that alveolar surface area changes very little during lung inflation. This and the average decrease in alveolar depth, *h*, in Fig. 3*A* suggest an accordion-like extension of alveolar ducts during lung inflation. This conclusion is supported by our previous ex vivo study in dog lungs where we observed an increase in alveolar depth during deflation (13) and by the observations of Macklin (17) and Klingele and Staub (14). However, this change in alveolar shape results in only a 19% increase in alveolar volume (see Fig. 3*B*) while the total lung volume increases by 143%. Based on these results, the small increase in alveolar volume cannot account for the large increase in total lung volume. In fact, our results in Fig. 3*D* show a large increase in the number of alveoli, on average from 293 million at RV + 1 to 572 million at TLC, suggesting that recruitment of new alveoli plays the more significant role in in vivo lung inflation in humans.

Table 2. *Statistical tests*

		Paired *t*-Tests		
	ANOVA	RV + 1 and TLC	FRC +1 and TLC	RV +1 and FRC +1
R	0.0004	0.005	0.008	0.02
h	10^{-5}	0.0002	0.008	0.001
V_a	0.0006	0.007	0.01	0.03
S_a	0.10	0.13	0.21	0.09
N_{tot}	10^{-6}	10^{-5}	0.002	0.005
ADC	10^{-6}	10^{-5}	0.001	0.01

P values for repeated-measures ANOVA and paired *t*-test pairwise comparisons between RV +1 and TLC, FRC +1 and TLC, and RV +1 and FRC +1 for *R, h,* V_a, S_a, N_{tot}, and anisotropic diffusion coefficients (ADC).

In calculating N_{tot}, we make a common assumption that alveoli are in one of two states: open (recruited) with gas volume V_a, or closed (derecruited) with zero gas volume. An alternate scenario might allow for the closed alveoli to have some small but nonzero trapped gas volume. If it is assumed that while in the closed state the closed alveoli have received no gas during inspiration, their volume would not affect the alveolar volume measured by ^{3}He lung morphometry. Thus, in this scenario, the value of n_a measured by ^{3}He lung morphometry is the number density of open alveoli only. On the other hand the total lung volume, measured from the proton images, would have a small contribution from the closed nonzero volume alveoli. Thus, using ^{3}He lung morphometry to calculate the total number of open alveoli as previously described ($N_{tot} = \bar{n}_a \cdot V_{tot}$) would lead to an overestimation of N_{tot}. This overestimation would be more significant at lower lung volumes where a greater fraction of alveoli are in the closed state, and the effect of recruitment would be understated by our method.

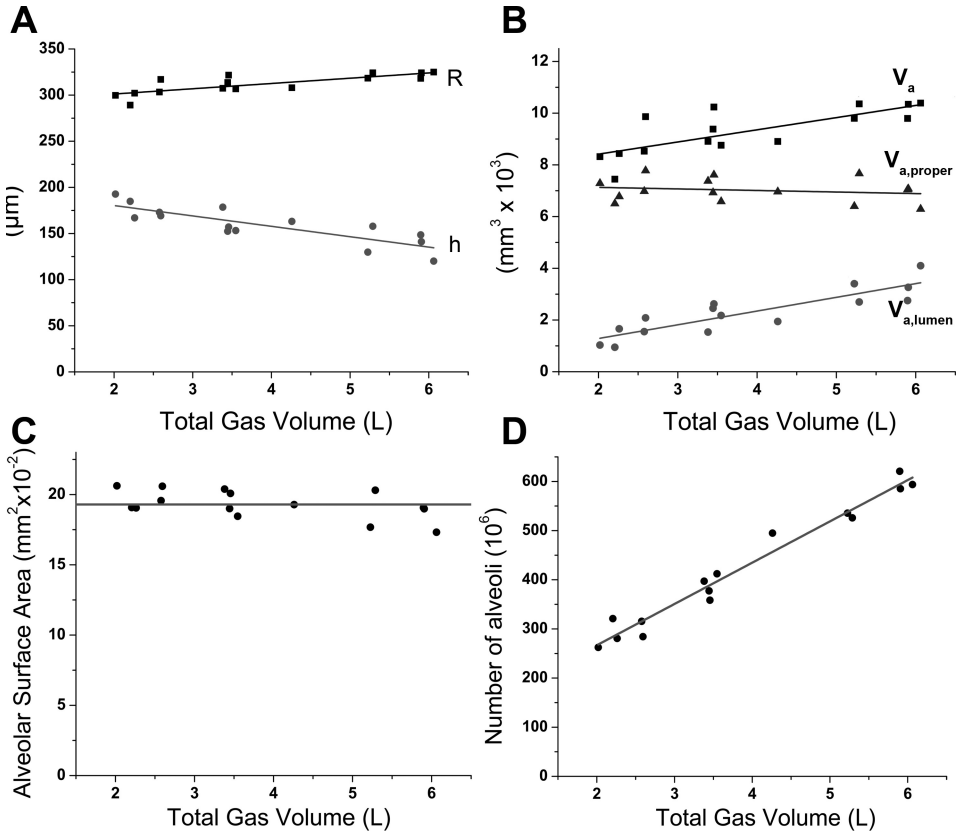

Fig. 3. Microgeometrical parameters obtained by ^{3}He lung morphometry plotted against total lung gas volume for 5 subjects. Each data point represents a parameters value averaged over the entire lung for one subject at a particular lung volume. *A*: plot of average alveolar duct radius, R, and alveolar depth, h, vs. total lung gas volume. Linear fits to the data give $R = 5.71V_{tot} + 290$ and $h = -11.3V_{tot} + 203$. *B*: plot of average alveolar volume, V_a, alveolar proper volume, $V_{a,prop}$, and one-eighth alveolar lumen volume, $V_{a,lumen}$, vs. total lung gas volume, V_{tot}. Linear fits to the data give $V_a = 0.47V_{tot} + 7.47$, $V_{a,proper} = -0.06V_{tot} + 7.25$, and $V_{a,lumen} = 0.53V_{tot} + 0.22$. *C*: plot of average alveolar surface area, S_a, vs. total lung gas volume, V_{tot}. A constant line fit to the data gives $S_a = 0.193$ mm^2. *D*: plot of total number of alveoli, N_{tot}, vs. total gas lung volume, V_{tot}. A linear fit to the data gives $N_{tot} = 98.8V_{tot} + 84.0$.

A common approach for analyzing alveolar mechanics relates the total alveolar surface area, S_{tot}, to total lung volume, V_{tot}, by the simple power function

$$S_{tot} = kV_{tot}^{n} \quad (9)$$

where k and n are constants (11). Greaves et al. (11) outline the relationship between possible values of n and each of the five previously mentioned mechanisms for lung inflation. Isotropic changes in alveolar dimensions would result in $n = 2/3$, "saucer-to-cup"-like change in alveolar shape would result in $n > 2/3$, "cup-to-saucer"-like change in the shape would result in $n < 2/3$, "accordion-like extension" would result in $n = 0$, and alveolar recruitment would result in $n = 1$. Using *Eq. 9* the authors summarize the results of several studies of lung micromechanics, but caution that while a given volume change mechanism results in a particular value of the exponent n, the converse is not true. A combination of several volume change mechanisms would result in an intermediate value of n.

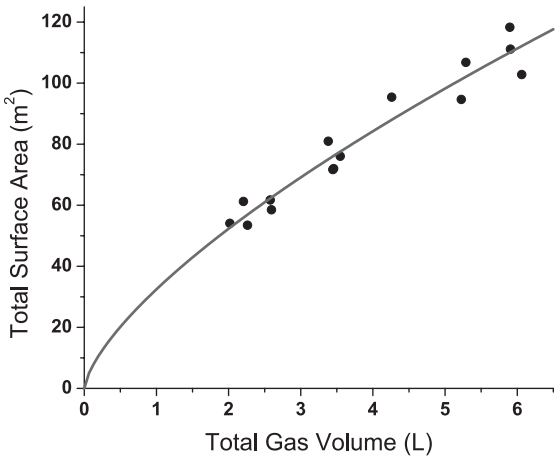

Fig. 4. Plot of total surface area, S_{tot}, vs. total lung volume, V_{tot}, for all 5 subjects at each of the 3 volumes TLC, FRC + 1, and RV + 1, with best fit curve for $S_{tot} = kV_{tot}^{n}$, ($n = 0.69 \pm 0.05$).

Perhaps this ambiguity in the interpretation of morphometric measurements explains some of the historical discrepancies in conclusions regarding lung micromechanics. Many of the early studies of pulmonary micromechanics concluded that alveoli expand isotropically based on surface area measurements determined by the mean linear intercept method (6, 7, 9). Fitting *Eq. 9* to their data, they obtained values of $n \approx 2/3$ and concluded that alveolar ducts expand isotropically. However, their findings could also be explained by a combination of alveolar recruitment ($n = 1$) and a "cup-to-saucer"-like change in the shape of alveolar ducts ($n < 2/3$). The relationship between total lung surface area and total lung volume does not, by itself, distinguish between these two possibilities. For example, fitting *Eq. 9* to our results for total lung surface area ($S_{tot} = N_{tot} \cdot S_a$) and total lung volume (Fig. 4) results in $n = 0.69 \pm 0.05$. This result agrees with results of Dunnill (7), Forrest (9), and D'Angelo (6). However, we also measure a large increase in N_{tot}, a decrease in alveolar depth, and constant alveolar surface area during lung inflation, indicating that the lung inflates by a combination of recruitment and accordion-like expansion of alveolar ducts rather than by isotropic expansion of alveoli.

While our current results may illuminate one source of previous disagreement regarding microstructural changes in

acinar airways, they do not resolve the issue completely. In our previous study of deflation in excised dog lungs, we observed that derecruitment plays a much less important role in ex vivo lung deflation and that changes in alveolar volume account for the bulk of change in total lung volume. This discrepancy suggests differences between species, a difference between inflation and deflation, or a difference between ex vivo and in vivo lung mechanics. Further studies of lung micromechanics with ^{3}He morphometry have the potential to investigate the significance of each of these factors.

Understanding the mechanisms for lung volume change in healthy lungs is necessary in order to understand lung malfunction due to disease and improper mechanical lung ventilation. Ventilator-induced lung injury (VILI) is a potential complication for patients undergoing mechanical ventilation. The causes of VILI are not fully understood, and understanding normal alveolar mechanics is the first step in determining ventilation strategies to limit VILI.

Using ^{3}He lung morphometry we have, for the first time, imaged precise in vivo morphological changes at the alveolar level during inspiration in five healthy human volunteers. The results indicate that in humans during inspiration alveolar duct radii increase only slightly, with a more significant decrease in alveolar depth, and a large increase in the number of alveoli. These findings suggest that, during inflation, the total lung volume increases largely by alveolar recruitment, with a smaller contribution from the increase in alveolar duct volume via anisotropic change of alveolar shape. We also show lung volume changes viewed only through the lens of standard morphological techniques could potentially be misinterpreted. This insight might help to resolve some of the apparent discrepancies between previous lung micromechanics studies.

ACKNOWLEDGMENTS

We express our gratitude to the late Peter Macklem for many helpful discussions and his pioneering work in the field.

GRANTS

This work was supported by National Heart, Lung, and Blood Institute Grants R01-HL-090806, R01-HL-7003701, and T32-HL-007317.

DISCLOSURES

No conflicts of interest, financial or otherwise, are declared by the author(s).

AUTHOR CONTRIBUTIONS

A.J.H. and J.C.W. conception and design of research; A.J.H., J.D.Q., and J.C.W. performed experiments; A.J.H., D.A.Y., and A.L.S. analyzed data; A.I.H., D.A.Y., M.S.C., and J.C.W. interpreted results of experiments; A.J.H. prepared figures; A.J.H. drafted manuscript; A.J.H., D.A.Y., A.L.S., J.D.Q., M.S.C., and J.C.W. edited and revised manuscript; A.J.H., D.A.Y., A.L.S., J.D.Q., M.S.C., and J.C.W. approved final version of manuscript.

REFERENCES

1. **Albert S, DiRocco J, Allen G, Bates J, Lafollette R, Kubiak B, Fischer J, Maroney S, Nieman G.** The role of time and pressure on alveolar recruitment. *J Appl Physiol* 106: 757–765, 2009.
2. **Armstrong JD, Gluck EH, Crapo RO, Jones HA, Hughes JM.** Lung tissue volume estimated by simultaneous radiographic and helium dilution methods. *Thorax* 37: 676–679, 1982.
3. **Bachofen H, Schürch S, Urbinelli M, Weibel ER.** Relations among alveolar surface tension, surface area, volume, and recoil pressure. *J Appl Physiol* 62: 1878–1887, 1987.
4. **Carney D, Bredenberg C, Schiller H, Picone A, McCann U, Gatto L, Bailey G, Fillinger M, Nieman G.** The mechanism of lung volume change during mechanical ventilation. *Am J Respir Crit Care Med* 160: 1697–1702, 1999.
5. **Chen X, Hedlund L, Möller H, Chawla M, Maronpot R, Johnson G.** Detection of emphysema in rat lungs by using magnetic resonance measurements of 3He diffusion. *Proc Natl Acad Sci USA* 97: 11478–11481, 2000.
6. **D'Angelo E.** Local alveolar size and transpulmonary pressure in situ and in isolated lungs. *Respir Physiol* 14: 251–266, 1972.
7. **Dunnill MS.** Effect of lung inflation on alveolar surface area in the dog. *Nature* 214: 1013–1014, 1967.
8. **Flicker E, Lee JS.** Equilibrium of force of subpleural alveoli: implications to lung mechanics. *J Appl Physiol* 36: 366–374, 1974.
9. **Forrest J.** The effect of changes in lung volume on the size and shape of alveoli. *J Physiol* 210: 533–547, 1970.
10. **Gierada DS, Woods JC, Bierhals AJ, Bartel ST, Ritter JH, Choong CK, Das NA, Hong C, Pilgram TK, Chang YV, Jacob RE, Hogg JC, Battafarano RJ, Cooper JD, Meyers BF, Patterson GA, Yablonskiy DA, Conradi MS.** Effects of diffusion time on short-range hyperpolarized (3)He diffusivity measurements in emphysema. *J Magn Reson Imaging* 30: 801–808, 2009.
11. **Greaves IA, Hildebrandt J, Hoppin FG.** Micromechanics of the lung. In: *Handbook of Physiology. The Respiratory System.* Bethesda, MD: Am. Physiol. Soc., 1986, vol. III, p. 217–231.
12. **Haefeli-Bleuer B, Weibel E.** Morphometry of the human pulmonary acinus. *Anat Rec* 220: 401–414, 1988.
13. **Hajari AJ, Yablonskiy DA, Quirk JD, Sukstanskii AL, Pierce RA, Deslée G, Conradi MS, Woods JC.** Imaging alveolar-duct geometry during expiration via ^{3}He lung morphometry. *J Appl Physiol* 110: 1448–1454, 2011.
14. **Klingele T, Staub N.** Alveolar shape changes with volume in isolated, air-filled lobes of cat lung. *J Appl Physiol* 28: 411–414, 1970.
15. **Lutey B, Lefrak S, Woods J, Tanoli T, Quirk J, Bashir A, Yablonskiy D, Conradi M, Bartel S, Pilgram T, Cooper J, Gierada D.** Hyperpolarized ^{3}He MR imaging: physiologic monitoring observations and safety considerations in 100 consecutive subjects. *Radiology* 248: 655–661, 2008.
16. **Macklem PT.** Respiratory mechanics. *Annu Rev Physiol* 40: 157–184, 1978.
17. **Macklin C.** Alveoli of mammalian lung: anatomical study with clinical correlation. *Proc Inst Med Chic* 18: 78–95, 1950.
18. **Mata JF, Altes TA, Cai J, Ruppert K, Mitzner W, Hagspiel KD, Patel B, Salerno M, Brookeman JR, de Lange EE, Tobias WA, Wang HT, Cates GD, Mugler JP.** Evaluation of emphysema severity and progression in a rabbit model: comparison of hyperpolarized ^{3}He and 129Xe diffusion MRI with lung morphometry. *J Appl Physiol* 102: 1273–1280, 2007.
19. **Osmanagic E, Sukstanskii AL, Quirk JD, Woods JC, Pierce RA, Conradi MS, Weibel ER, Yablonskiy DA.** Quantitative assessment of lung microstructure in healthy mice using an MR-based 3He lung morphometry technique. *J Appl Physiol* 109: 1592–1599, 2010.
20. **Patz S, Muradian I, Hrovat MI, Ruset IC, Topulos G, Covrig SD, Frederick E, Hatabu H, Hersman FW, Butler JP.** Human pulmonary imaging and spectroscopy with hyperpolarized ^{129}Xe at 0.2T. *Acad Radiol* 15: 713–727, 2008.
21. **Patz S, Muradyan I, Hrovat M, Dabaghyan M, Washko G, Hatabu H, Butler J.** Diffusion of hyperpolarized 129Xe in the lung: a simplified model of 129Xe septal uptake and experimental results. *New J Physics* 13: 2011.
22. **Peces-Barba G, Ruiz-Cabello J, Cremillieux Y, Rodríguez I, Dupuich D, Callot V, Ortega M, Rubio Arbo M, Cortijo M, Gonzalez-Mangado N.** Helium-3 MRI diffusion coefficient: correlation to morphometry in a model of mild emphysema. *Eur Respir J* 22: 14–19, 2003.
23. **Quirk JD, Lutey BA, Gierada DS, Woods JC, Senior RM, Lefrak SS, Sukstanskii AL, Conradi MS, Yablonskiy DA.** In vivo detection of acinar microstructural changes in early emphysema with ^{3}He lung morphometry. *Radiology* 260: 866–874, 2011.
24. **Rodriguez M, Bur S, Favre A, Weibel ER.** Pulmonary acinus: geometry and morphometry of the peripheral airway system in rat and rabbit. *Am J Anat* 180: 143–155, 1987.
25. **Saam B, Yablonskiy D, Kodibagkar V, Leawoods J, Gierada D, Cooper J, Lefrak S, Conradi M.** MR imaging of diffusion of ^{3}He gas in healthy and diseased lungs. *Magn Reson Med* 44: 174–179, 2000.
26. **Storey W, Staub N.** Ventilation of terminal air units. *J Appl Physiol* 17: 391–397, 1962.

27. **Sukstanskii A, Yablonskiy D.** In vivo lung morphometry with hyperpolarized ^{3}He diffusion MRI: theoretical background. *J Magn Reson* 190: 200–210, 2008.
28. **Sukstanskii AL, Bretthorst GL, Chang YV, Conradi MS, Yablonskiy DA.** How accurately can the parameters from a model of anisotropic ^{3}He gas diffusion in lung acinar airways be estimated? Bayesian view. *J Magn Reson* 184: 62–71, 2007.
29. **Tsunoda S, Fukaya H, Sugihara T, Martin CJ, Hildebrandt J.** Lung volume, thickness of alveolar walls, and microscopic anisotropy of expansion. *Respir Physiol* 22: 285–296, 1974.
30. **Wang W, Nguyen NM, Yablonskiy DA, Sukstanskii AL, Osmanagic E, Atkinson JJ, Conradi MS, Woods JC.** Imaging lung microstructure in mice with hyperpolarized ^{3}He diffusion. *MRI Magn Reson Med* 65: 620–626, 2011.
31. **West JB.** *Respiratory Physiology—The Essentials*. Baltimore, MD: Williams and Wilkins, 1995, p. xii.
32. **Woods J, Choong C, Yablonskiy D, Bentley J, Wong J, Pierce J, Cooper J, Macklem P, Conradi M, Hogg J.** Hyperpolarized ^{3}He diffusion MRI and histology in pulmonary emphysema. *Magn Reson Med* 56: 1293–1300, 2006.
33. **Yablonskiy D, Sukstanskii A, Leawoods J, Gierada D, Bretthorst G, Lefrak S, Cooper J, Conradi M.** Quantitative in vivo assessment of lung microstructure at the alveolar level with hyperpolarized ^{3}He diffusion MRI. *Proc Natl Acad Sci USA* 99: 3111–3116, 2002.
34. **Yablonskiy D, Sukstanskii A, Woods J, Gierada D, Quirk J, Hogg J, Cooper J, Conradi M.** Quantification of lung microstructure with hyperpolarized 3He diffusion MRI. *J Appl Physiol* 107: 1258–1265, 2009.